Acta Astronautica 67 (2010) 623–638

Contents lists available at ScienceDirect

Acta Astronautica

journal homepage: www.elsevier.com/locate/actaastro

Chaining periodic three-body orbits in the Earth–Moon system

Jeffrey S. Parker *,[1], Kathryn E. Davis, George H. Born

The Colorado Center for Astrodynamics Research, University of Colorado, Boulder, CO 80309, USA

ARTICLE INFO

Article history:
Received 25 August 2009
Received in revised form
24 March 2010
Accepted 2 April 2010

Keywords:
Earth–Moon orbits
Three-body trajectories
Low-energy
Mission design
Dynamical systems
Manifolds
Orbit transfers

ABSTRACT

In this paper, we describe methods to construct complex chains of orbit transfers in the planar circular restricted Earth–Moon three-body system using the invariant manifolds of unstable three-body orbits. It is shown that the Poincaré map is a useful tool to identify and construct transfer trajectories from one orbit to another, i.e., homoclinic and heteroclinic orbit connections, with applications to practical spacecraft mission design. A multiple-shooting differential corrector is used to construct complex orbit chains and complex periodic orbits. The resulting complex periodic orbits are shown to be members of continuous families of such orbits, where the characteristics of each orbit in the family vary continuously from one end of the family to the other. Finally, we characterize the cost of constructing an orbit transfer between any two points along two libration orbits using a single maneuver. It is shown that a spacecraft requires substantially less ΔV to perform such single-maneuver transfers if the transfers are near heteroclinic connections in the corresponding phase space.

© 2010 Elsevier Ltd. All rights reserved.

1. Introduction

NASA has called for a sustained, evolutionary approach to the development of lunar exploration. This approach will certainly call for a variety of mission designs, including the placement of satellites in low lunar orbits as well as in higher communication and navigation orbits. Recent studies have considered the advantages of placing a communication/navigation satellite in a three-body orbit, such as a halo orbit or other libration orbit [1–3]. Furthermore, there are distinct advantages with placing several satellites in different orbits, where the satellites operate as a constellation and would likely share the same launch vehicle. It would be desirable if the satellites could transfer into their various orbits without expending a large amount of fuel to do so. In this paper, we present methods to construct low-energy orbit transfers between unstable three-body orbits such as libration orbits. It is shown that simple three-body orbits may be chained together to construct complicated mission itineraries that spacecraft may follow using very little fuel. This work may be applied to the design of practical spacecraft missions, including the design of orbit transfers for communication and navigation satellites, the construction of rendezvous trajectories, or the design of the trajectories needed to deploy a constellation of satellites in different orbits from a single launch vehicle. The methods described here are applicable to many three-body systems, though this study focuses on the Earth–Moon three-body system.

This paper is organized in the following manner. Section 2 provides the necessary background of the dynamical systems methodology used here. Section 3 demonstrates how to use this methodology to construct low-energy transfers from one unstable three-body orbit to another. Section 4 then discusses how to construct complicated orbit chains from simple periodic orbits. In reality, practical spacecraft mission designs have additional constraints that may restrict what transfers are available. For instance, the spacecraft may not have enough time to perform a free transfer and must perform a small maneuver to hasten the transfer. Section 5 characterizes the cost and benefits of transferring from

* Corresponding author. Tel.: +1 303 931 5334.
E-mail addresses: parkerjs@gmail.com (J.S. Parker), katedavis22@gmail.com (K.E. Davis), george.born@colorado.edu (G.H. Born).
[1] Currently at the Jet Propulsion Laboratory, California Institute of Technology, 4800 Oak Grove Dr., Pasadena, CA 91109, USA.

0094-5765/$ - see front matter © 2010 Elsevier Ltd. All rights reserved.
doi:10.1016/j.actaastro.2010.04.003

one unstable three-body orbit to another using a single maneuver. Finally, Section 7 discusses several applications of this research to practical lunar mission designs.

2. Background

This section includes a description of the aspects of dynamical systems theory that have been used in the development of low-energy orbit transfers and orbit chains.

2.1. Circular restricted three-body problem (CRTBP)

The trajectories produced in this paper have been propagated in the model formulated by the circular restricted three-body problem (CRTBP) [4]. The model is used to characterize the motion of a massless particle, e.g., a spacecraft, in the presence of two massive bodies, e.g., the Earth and the Moon. The model assumes the two massive bodies orbit their barycenter in circular orbits.

It is convenient to characterize the motion of the third body, i.e., the spacecraft, in a reference frame that rotates at the same rate as the orbital motion of the two primary masses. The coordinate frame is centered at the barycenter of the system and oriented such that the x-axis extends from the barycenter toward the smaller primary, the z-axis extends toward the primary bodies' orbit normal, and the y-axis completes the right-handed coordinate frame. In that synodic frame, the two massive bodies are stationary and the spacecraft moves about the system in non-Keplerian motion. The equations of motion and additional information about the CRTBP may be found in the literature [4,5].

The dynamics of the CRTBP permit an integral of motion to exist in the synodic reference frame, known as the Jacobi integral or Jacobi constant [5–7]. The Jacobi constant of a spacecraft in a three-body system may be written simply as

$$C = 2U - V^2 \quad \text{where} \tag{1}$$

$$U = \frac{1}{2}(x^2+y^2) + \frac{1-\mu}{r_1} + \frac{\mu}{r_2} \tag{2}$$

$$V^2 = \dot{x}^2 + \dot{y}^2 + \dot{z}^2 \tag{3}$$

$$r_1^2 = (x+\mu)^2 + y^2 + z^2 \tag{4}$$

$$r_2^2 = (x+\mu-1)^2 + y^2 + z^2 \tag{5}$$

The spacecraft's position and velocity coordinates are given in normalized synodic coordinates [4]; the parameter μ is the three-body constant, computed for the Earth–Moon system by dividing the Moon's mass by the total mass in the system, which yields a value of approximately 0.012150604. The Jacobi constant of a spacecraft moving in the CRTBP may not change unless the spacecraft is perturbed in some way other than by the gravitational attraction of the two primary bodies.

There are five well-known equilibrium solutions to the CRTBP, known as the five Lagrange, or libration points [4]. These points are referred to as L_1–L_5; this paper adopts the nomenclature that L_1 lies between the two primary masses and L_2 lies on the far side of the smaller primary, relative to the barycenter of the system. The Lagrange points in the Earth–Moon system are abbreviated in this study using the nomenclature $LL_1 - LL_5$.

2.2. Periodic orbits in the CRTBP

The CRTBP permits the existence of numerous families of periodic and quasiperiodic orbits; examples of orbits in many of these families may be found in numerous papers, dating back to the 1890s [5,8–22]. Several orbits that have interesting applications to practical spacecraft missions in the near-Earth environment include distant prograde orbits about the Moon and libration orbits about LL_1 and LL_2. Families of these orbits exist in both two and three dimensions [5,17–22]. The planar families of simple periodic libration orbits are known as Lyapunov orbits. Several example orbits from these three planar families of unstable three-body orbits are shown in Fig. 1.

The CRTBP permits an infinite number of families of periodic orbits, a statement that will be verified in this paper. Many authors have worked to categorize these families [9,11,17]. Strömgren defined the classification of *simple periodic orbits* to be three-body orbits that pierce the x-axis exactly two times per orbit and are symmetric about the $x-z$ plane [9]. Both piercings necessarily occur in an orthogonal manner. These orbits exist due to the invariance of the equations of motion to the transformations $t' = -t$ and $y' = -y$. Each orbit shown in Fig. 1 is an example of a simple periodic orbit using this definition. This paper uses simple periodic orbits as building blocks to generate complex trajectories in the Earth–Moon system.

A symmetric orbit may be uniquely represented by one of its orthogonal x-axis crossings using either the state $[x_0, z_0, \dot{y}_0]$ or the simpler state $[x_0, C]$, provided that only one orbit exists in the given family for each value of the Jacobi constant [20]. Fig. 2 shows plots of the initial conditions of orbits in the family of planar LL_1 Lyapunov orbits, where the initial conditions have been specified at the x-axis crossing with a positive $\dot{y}$ value. One can see that the family extends from a point where the first x-axis crossing passes just above the Earth, corresponding to a very large Lyapunov orbit, to a point where the x-axis crossing encounters the L_1 point, corresponding to a very small Lyapunov orbit about L_1. Theoretical Lyapunov orbits also exist that pierce the surface of the Earth; they will not be considered in this paper for practical reasons.

A symmetric orbit, such as a Lyapunov orbit, may be represented by two variables, e.g., x_0 and C; a third parameter τ may then be used to specify the location of a body along that orbit. In this paper, τ is represented as a revolution number, such that τ begins at a value of zero at the orbit's initial state and advances linearly in time until it reaches a value of one upon arriving at the same state. This is a particularly useful way to parameterize the state along a three-body orbit when the orbit requires several

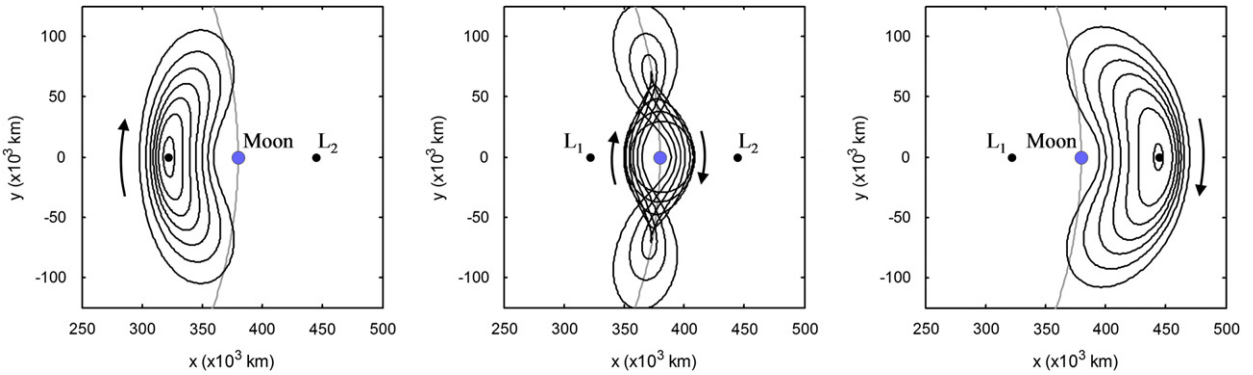

Fig. 1. Several example orbits from three families of unstable periodic Earth–Moon three-body orbits, viewed from above in the Earth–Moon synodic reference frame. The orbits shown are from the family of Lyapunov orbits about L_1 (left), the family of distant prograde orbits about the Moon (center), and the family of Lyapunov orbits about L_2 (right). The arrows indicate the motion of objects traversing these orbits; the Moon's orbital radius about the Earth–Moon barycenter is shown in gray for reference.

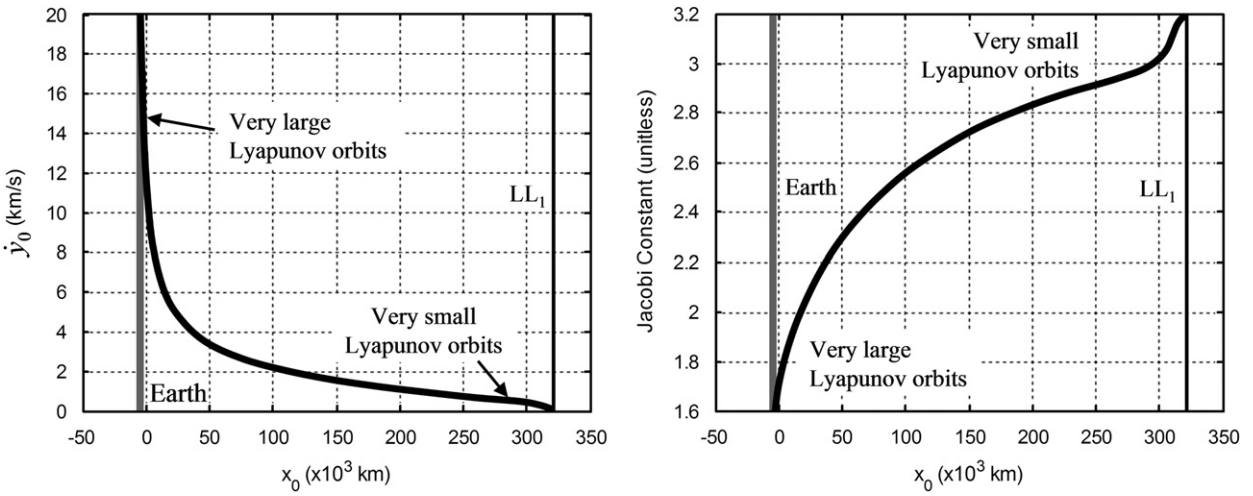

Fig. 2. Plots of $\mathbf{x_0}$ vs. $\dot{\mathbf{y}}_\mathbf{0}$ (left) and $\mathbf{x_0}$ vs. **C** (right) for the family of Lyapunov orbits about the Earth–Moon L_1 point. The initial values of the other cartesian coordinates are all equal to zero for each orbit in this family.

revolutions to close. Fig. 3 shows an example of how τ advances in time about an LL_2 Lyapunov orbit.

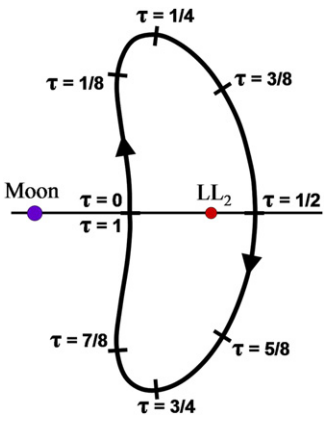

Fig. 3. An illustration of the progression of τ about a planar LL_2 Lyapunov orbit.

2.3. Invariant manifolds

Theoretically, a particle with a perfectly specified state will remain on an unstable orbit indefinitely [23]. In reality, the state of a spacecraft following an unstable orbit in the presence of any random perturbation will exponentially diverge over time from its nominal state along the orbit. The station-keeping costs for spacecraft on unstable trajectories in the Sun–Earth three-body system have been on the order of 1 m/s per month or less [24–27]. One advantage of unstable trajectories becomes obvious when a spacecraft's mission calls for it to depart its orbit and transfer to a new orbit. In such cases, the unstable nature of three-body orbits enables low-energy transfers.

An orbit's *unstable invariant manifold* (W^U) contains the set of all trajectories that a particle will take if it is perturbed anywhere on that orbit in the direction of the orbit's local unstable eigenvector [7,28]. Similarly, an orbit's *stable invariant manifold* (W^S) contains the set of all

trajectories that a particle may take to asymptotically arrive onto that orbit along the orbit's local stable eigenvector. Put another way, the orbit's stable invariant manifold is the set of all trajectories that a particle will take backward through time if it is perturbed in the direction of the orbit's local stable eigenvector. The invariant manifolds of periodic orbits in the CRTBP have *interior* and *exterior* halves, where, for instance, the trajectories in the interior half of a Lyapunov orbit's manifold immediately approach the interior of the system and vice versa. Fig. 4 shows plots of the stable and unstable invariant manifolds of an example Lyapunov orbit about the Earth–Moon L_2 point. The interior manifold in each case propagates toward the Moon; the exterior manifold traverses away from the Earth and the Moon.

In practice, mission designers model an orbit's stable and unstable invariant manifolds by taking states along the orbit, perturbing them in an appropriate way, and integrating the resulting set of states through time [5,29,30]. The initial conditions $\mathbf{X}_0^S$ and $\mathbf{X}_0^U$ for the trajectories that may be used to model an orbit's stable and unstable manifolds, respectively, may be constructed using the following equations:

$$\mathbf{X}_0^S = \mathbf{X}_0 \pm \varepsilon \frac{\mathbf{v}^S}{|\mathbf{v}^S|} \quad \text{and} \quad \mathbf{X}_0^U = \mathbf{X}_0 \pm \varepsilon \frac{\mathbf{v}^U}{|\mathbf{v}^U|} \tag{6}$$

where $\mathbf{v}^S$ and $\mathbf{v}^U$ are the stable and unstable eigenvectors of the orbit's local state transition matrix, respectively, ε is the magnitude of the perturbation, and the sign of the perturbation differentiates between the interior and exterior halves of the orbit's manifolds. It is common to normalize the perturbations across the entire manifold such that the perturbations have a constant position magnitude, e.g., 100 km [31]. This perturbation does slightly change the trajectory's Jacobi constant value.

As ε in Eq. (6) is reduced to zero, the resulting trajectories more precisely model the orbit's manifold, however, it takes more propagation time for the trajectories to depart the host orbit. This study assumes that in practice a spacecraft approaching an Earth–Moon three-body orbit along its stable manifold has arrived on the orbit once its state is within 100 km of the orbit; ε is therefore set to provide a normalized perturbation with a position magnitude of 100 km.

2.4. Homoclinic and heteroclinic connections

Many unstable periodic orbits in the CRTBP contain *homoclinic* connections with themselves and/or *heteroclinic* connections with other unstable periodic orbits [7,32,33]. If a trajectory in an orbit's unstable manifold departs that orbit, traverses the three-body system for some time, and then later arrives back onto the same orbit, it makes what is known as a homoclinic connection with the host orbit [32]. This trajectory is contained within both the orbit's unstable and stable manifolds. McGehee proved the existence of homoclinic connections in both the interior and exterior regions of the three-body system [34]. In a similar sense, a different trajectory within the unstable manifold of one orbit may depart that orbit and eventually arrive onto a second orbit. The trajectory is thus contained within both the unstable manifold of the first orbit and the stable manifold of the second orbit. Such a trajectory forms what is known as a heteroclinic connection between the two unstable orbits [32].

A heteroclinic transfer constructed in this paper includes the trajectory segment between the initial departure point from the first orbit, namely, the perturbed state $\mathbf{X}_0^U$ corresponding to τ^U, and the final arrival point at the second orbit, namely, the perturbed state $\mathbf{X}_0^S$ corresponding to τ^S. In this way, the duration of one orbit transfer generated in this paper may be directly compared with the duration of another transfer, knowing that each transfer begins and ends at a state 100 km away from the corresponding three-body orbit.

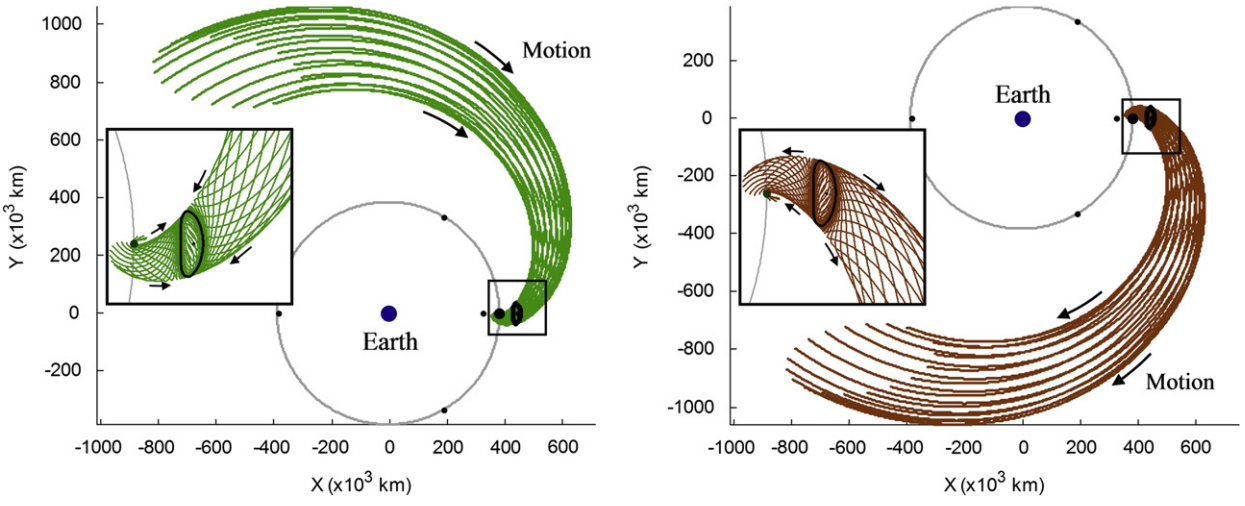

Fig. 4. The stable (left) and unstable (right) manifolds of a Lyapunov orbit about the Earth–Moon L_2 point, viewed from above in the Earth–Moon synodic reference frame.

Many authors have explored homoclinic and heteroclinic transfers between three-body orbits as transport mechanisms for spacecraft and comets [7,29,32,35–38]. Using dynamical systems theory, Lo and Ross noted that the orbit of the comet Oterma appeared to shadow the invariant manifolds of libration orbits about the L_1 and L_2 points in the Sun–Jupiter three-body system [39]. Koon et al. later showed that the comet closely followed a homoclinic–heteroclinic chain [32]. Gómez et al. began exploring the numerical construction of orbits with prescribed itineraries to describe the resonant transitions exhibited by the comet Oterma [7]. The material presented in this paper extends their work, applying a new method for the construction of prescribed orbit transfers in the Earth–Moon system.

2.5. Differential correction

A multiple-shooting differential corrector is used in this paper to link many unstable trajectory segments together to form a single, fully continuous trajectory. This differential corrector may be characterized as an iterative algorithm, where each iteration involves two levels of differential correction. The algorithm is described in detail in the literature [20,21,40].

2.6. Poincaré maps

A Poincaré map is a useful tool for analyzing dynamical systems and is used in this research to identify useful orbit transfers. A Poincaré map is created by intersecting a trajectory in the n-dimensional flow $\dot{\mathbf{x}} = f(\mathbf{x})$ by an $(n-1)$-dimensional surface of section Σ. Thus, the Poincaré mapping replaces the flow of an n th order system with a discrete system of order $(n-1)$ [41]. A Poincaré mapping, P, may be described as a function that maps the state of a trajectory at the k th intersection with the surface of section, $\mathbf{x}_k$, to the next intersection, $\mathbf{x}_{k+1}$

$$\mathbf{x}_{k+1} = P(\mathbf{x}_k) \tag{7}$$

If a trajectory pierces Σ at the state $\mathbf{x}^*$ at time t and then returns to $\mathbf{x}^*$ at time $t+T$, then one may conclude that the trajectory is a periodic orbit with a period T [23].

There are three different types of Poincaré maps considered in this research, defined as follows [23]:

- P_+: The Poincaré map created from only the positive intersections of the trajectory with the surface of section. For instance, in the CRTBP, Σ may be defined as a $y-z$ plane set to some x-value and P_+ includes only those intersections that have positive values of $\dot{x}$.
- P_-: The Poincaré map created from only the negative intersections of the trajectory with the surface of section.
- $P_\pm$: The Poincaré map created from all intersections of the trajectory with the surface of section.

The maps P_+ and P_- are called one-sided maps, while $P_\pm$ is called a two-sided map [23]. Fig. 5 provides a simple illustration of a one-sided Poincaré mapping of two orbits,

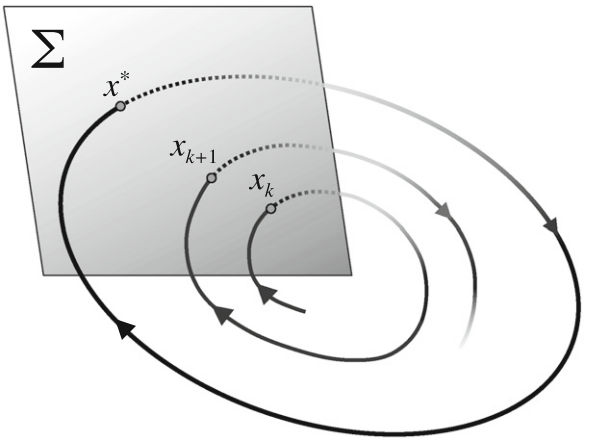

Fig. 5. An illustration of a one-sided Poincaré mapping of two trajectories. The point $\mathbf{x}^*$ indicates a fixed point on the surface, corresponding to a periodic trajectory.

where one is periodic and one is not immediately periodic.

3. Building free transfers/heteroclinic connections

Free transfers between unstable orbits may be located in the CRTBP by analyzing Poincaré maps [38]. Suppose there are two unstable Lyapunov orbits in the Earth–Moon three-body system: one about LL_1 and the other about LL_2. Both of these orbits have a set of stable and unstable invariant manifolds. In the planar CRTBP, each point along a manifold may be characterized by a four-dimensional state $[x,y,\dot{x},\dot{y}]$. If a surface of section is placed in $\mathbb{R}^4$ at some x-position, the resulting intersection is a surface in $\mathbb{R}^3$. If it is further specified that the two Lyapunov orbits have the same Jacobi constant, then each point along any trajectory within both orbits' manifolds will have the same Jacobi constant and the phase space of the problem is reduced to $\mathbb{R}^2$. The state at any intersection in the surface may only be reconstructed if the Poincaré map is one-sided, since the Jacobi constant has a sign ambiguity. The stable and unstable manifolds of both orbits appear as curves in the two-dimensional Poincaré map. Any intersection of these curves corresponds to a free transfer between the two orbits.

Fig. 6 illustrates the process of identifying free transfers from a Lyapunov orbit about LL_1 to a Lyapunov orbit about LL_2. In this case, the value of the Jacobi constant of both orbits has been selected to be 3.13443929. A P_+ Poincaré map has been constructed, where the surface Σ has been placed at the x-coordinate of the Moon, namely, at a value of approximately 379,730 km with respect to the barycenter of the Earth–Moon system. The left side of Fig. 6 illustrates the unstable and stable manifolds integrated to the first intersection with the surface of section. The intersection of both manifolds with the surface of section is shown in the right side of Fig. 6. One can see that there are two intersections that correspond to the two free transfers indicated in the figure.

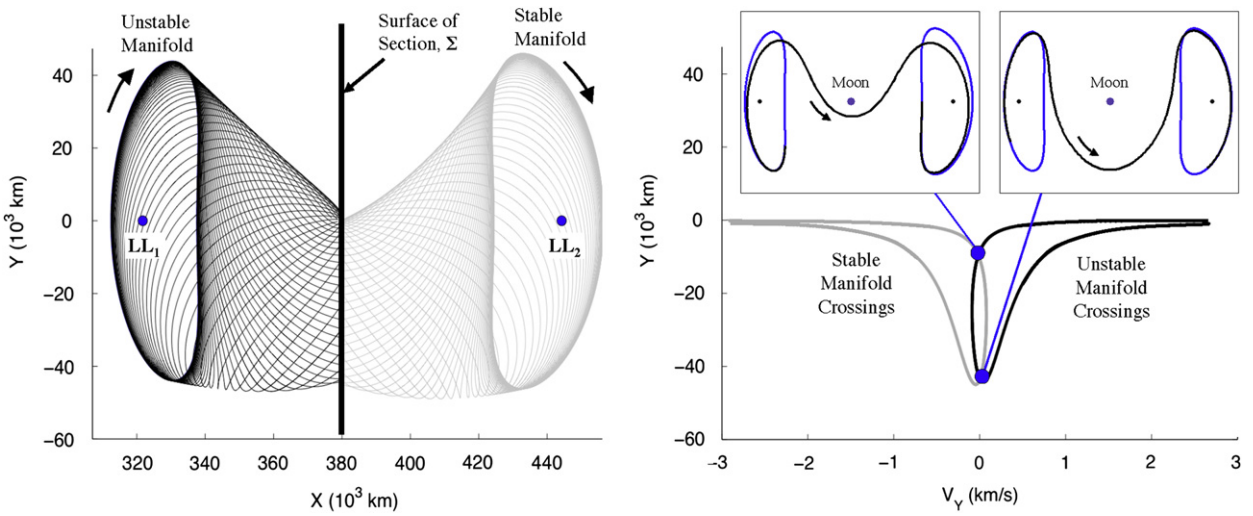

Fig. 6. An illustration of the process of using a Poincaré map to identify free transfers between two Lyapunov orbits. Both orbits have a Jacobi constant of 3.13443929. Left: the unstable manifold of an LL_1 Lyapunov orbit and the stable manifold of an LL_2 Lyapunov integrated to the surface of section; Right: the corresponding P_+ Poincaré map and two free transfers.

The simple illustration shown in Fig. 6 may be extended by propagating the manifolds longer and identifying intersections in the manifolds that correspond to longer, more complicated heteroclinic connections. The Poincaré map shown in Fig. 7 is produced by propagating the unstable manifold of the LL_1 Lyapunov orbit and the stable manifold of the LL_2 Lyapunov orbit for 60 days each. In addition, the map shown in Fig. 7 is a $P_{\pm}$ map, displaying all intersections of both manifolds with the surface of section. In this particular mapping, the majority of the points shown below the y=0 line are members of the P_+ map (including the points shown in Fig. 6), the majority of the points shown above it are members of the P_- map, and all observed intersections of the two manifolds do indeed intersect, even accounting for the sign ambiguity of $\dot{x}$.

Fig. 7 includes eight example orbit transfers to illustrate what sort of heteroclinic connections exist between these two libration orbits. Certain types of motion appear in more than one heteroclinic connection. For example, the trajectories labeled (1), (2), and (7) appear to graze a distant prograde orbit, whereas the trajectories labeled (1), (3), and (4) appear to traverse a figure-eight type orbit. The appearance of such orbits in the Poincaré maps reinforces the idea that one may construct a specific chain of simple orbits to construct a complicated itinerary of orbit transfers.

The Poincaré map is a useful tool to identify what sorts of orbit transfers exist, but it does not immediately reveal the shape or geometry of the transfers. For instance, the transfer labeled (8) in Fig. 7 includes a lunar flyby, which may or may not be desirable. Section 4 introduces a method that may be used to construct a desirable sequence of orbit transfers after identifying that such orbit transfers exist.

Free transfers only exist in the CRTBP between two unstable orbits that have the same Jacobi constant. Fig. 8 shows a plot of several families of three-body orbits in the Earth–Moon CRTBP, where the orbits' Jacobi constant values are plotted as functions of their x_0-values. The curves shaded in black correspond to unstable three-body orbits; the curves shaded in gray correspond to orbits that are neutrally stable [23]. The horizontal line indicates the Jacobi constant value used to produce the heteroclinic connections observed in Figs. 6 and 7. The figure verifies that the families of Lyapunov orbits about LL_1 and LL_2 both include unstable orbits at the same indicated Jacobi constant value, along with the family of distant prograde orbits, which helps to explain the appearance of such an orbit in the transfers labeled (1), (2), and (7) in Fig. 7.

4. Building complex orbit chains

In Section 3, a technique was presented that may be used to identify the heteroclinic connections between two unstable periodic orbits. Previous papers have theorized using symbolic dynamics that if a heteroclinic connection exists, it is possible to find a trajectory that transfers back and forth arbitrarily between those orbits. Robinson provides a thorough review of the background of symbolic dynamics [42]. Canalias et al. provide a methodology to search for a combination of homoclinic transfers that may be used to change the phase of a spacecraft traversing an unstable periodic orbit [37]. In this section we study a practical method to construct a complex orbit chain given a desired sequence of homoclinic and/or heteroclinic transfers.

4.1. Constructing a complex orbit chain

One may describe a spacecraft's itinerary between simple periodic orbits in the CRTBP by considering its state at each x-axis crossing. A spacecraft traversing any

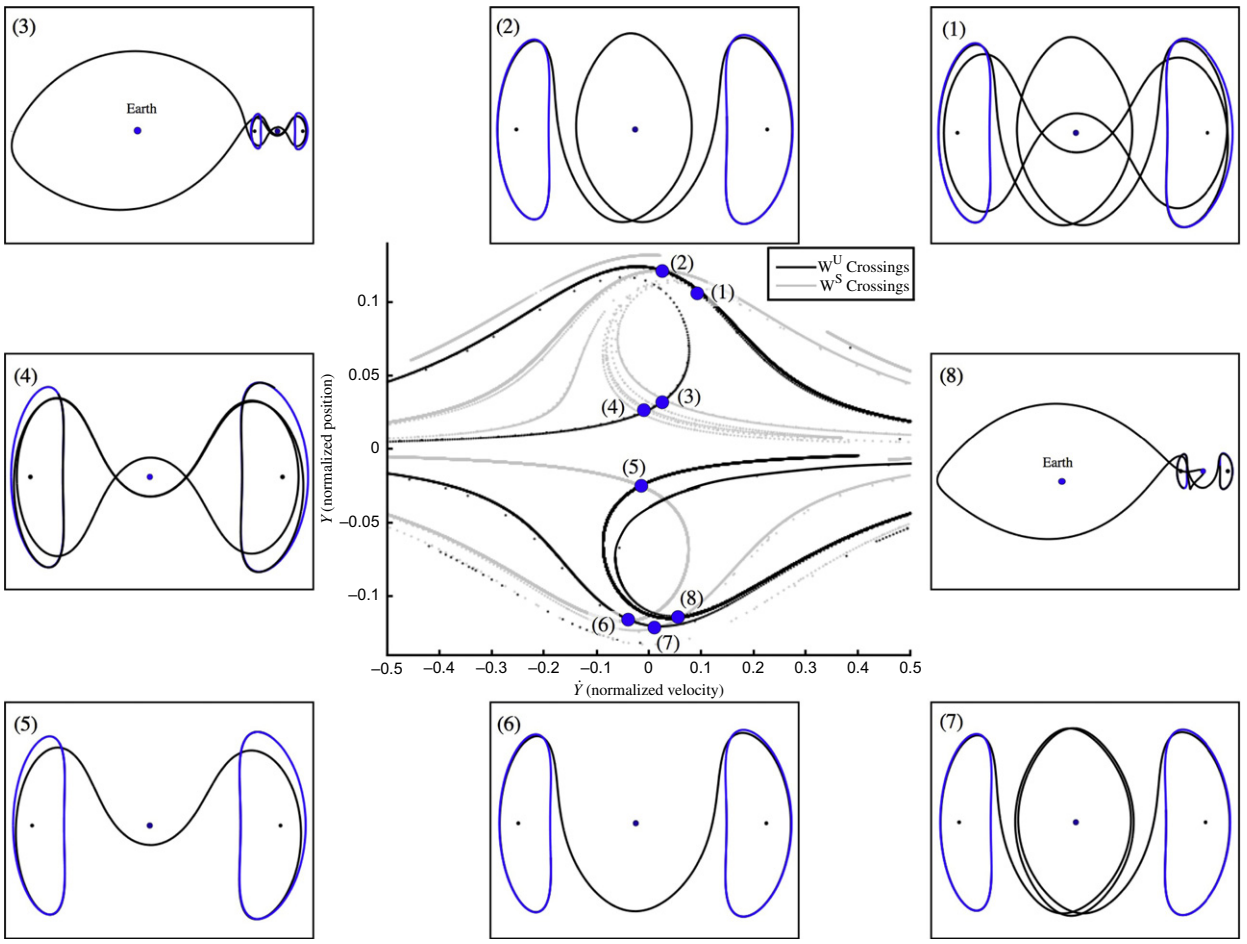

Fig. 7. The $P_{\pm}$ Poincaré map produced from the same system and surface of section shown in Fig. 6, now with an extended manifold propagation duration of 60 days. The plots shown surrounding the Poincaré map illustrate several example free transfers that have been identified in the map.

simple periodic orbit pierces the x-axis twice: once with positive and once with negative values of $\dot{y}$. One may model a simplified orbit transfer by considering that the spacecraft departs the initial orbit at one x-axis crossing, is midway through the transfer at the next x-axis crossing, and completes the transfer at a later x-axis crossing. Using this conceptualization, one may construct a set of x-axis states to describe a given itinerary between two orbits. A set of eight states are summarized in Fig. 9 and Table 1 for transfers between an example LL_1 Lyapunov orbit and an example distant prograde orbit that have the same Jacobi constant.

The states given in Fig. 9 and Table 1 have been collected from two sources. The states corresponding to the simple periodic orbits (A, B, E, and F) have been taken directly from those orbits; the algorithm described by Howell is well-suited to generate the states of a periodic orbit at their orthogonal x-axis crossings [20]. The states that correspond to the orbit transfers (C, D, G, and H) have been taken from their heteroclinic connections identified using the Poincaré analysis described in Section 3. A theoretical heteroclinic connection between these orbits asymptotically wraps off one orbit and onto the next as ε in Eq. (6) approaches 0; an infinite number of x-axis crossings precede the theoretical heteroclinic connection. The states D and H correspond to the x-axis crossings that are furthest from either host orbit. The states C and G correspond to the previous respective x-axis crossing. As one can see in Table 1, state C is approximately 306 km and 0.8 m/s away from state A and state G is approximately 2058 km and 28.9 m/s away from state E; these state differences are small enough to proceed without difficulty.

The states summarized in Fig. 9 and Table 1 may be used to construct a sequence of states that represent any itinerary between the two given orbits. This sequence may then be converted into a series of patchpoints that may be inputted to a differential corrector in order to produce a continuous trajectory. For instance, the trajectory of a spacecraft in orbit about the LL_1 Lyapunov orbit may be represented by the sequence

$$\{\ldots, A, B, A, B, \ldots\} \tag{8}$$

A differential corrector may be used to convert this sequence into a continuous trajectory. If a mission designer wishes to transfer the spacecraft from the LL_1

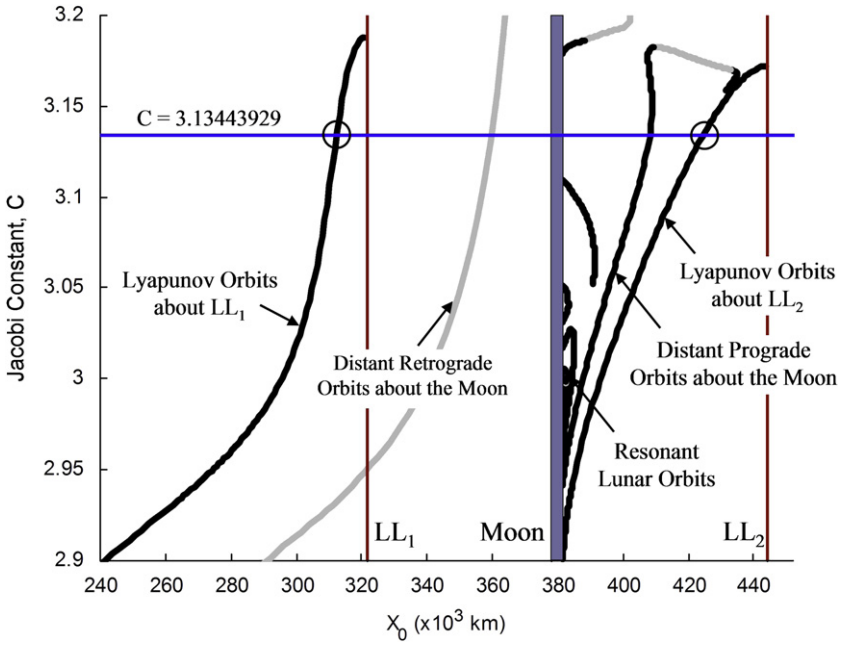

Fig. 8. A plot of several families of three-body orbits in the Earth–Moon CRTBP, where the orbits' Jacobi constant values are plotted as functions of their $\mathbf{x_0}$-values. The curves shaded in black correspond to unstable three-body orbits; the curves shaded in gray correspond to orbits that are neutrally stable [23].

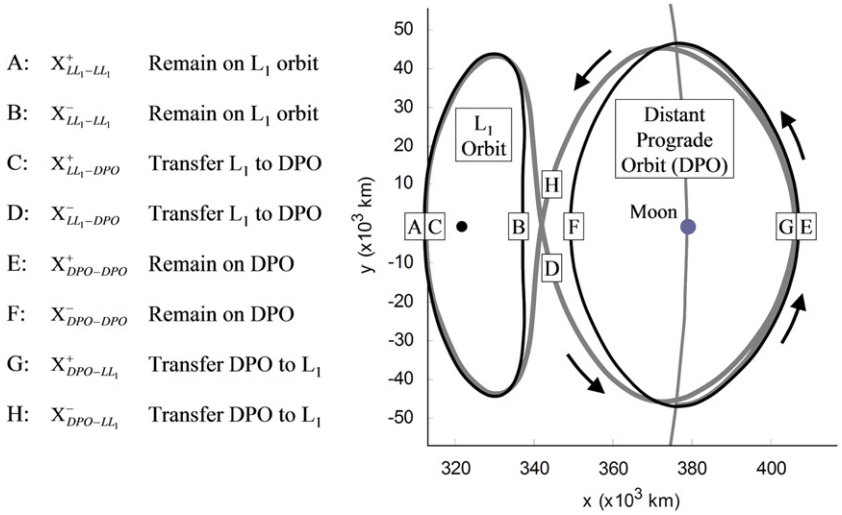

Fig. 9. A summary of the states needed to produce complex itineraries between two orbits. In this case, the two orbits are a Lyapunov orbit about L_1 and a distant prograde orbit (DPO) about the Moon. The states "D" and "H" are on the *x*-axis, although the labels are offset.

orbit to the distant prograde orbit, the designer would construct the sequence

$$\{\ldots,A,B,A,B,C,D,E,F,E,F,\ldots\} \tag{9}$$

and input that sequence into the differential corrector. The differential correction process adjusts every state in the sequence to accommodate the slight differences between the states A and C to make the transfer continuous.

Table 2 provides two example sequences that may be used as inputs to a differential corrector in order to produce continuous trajectories with different itineraries. To demonstrate this process, the first sequence in Table 2 has been converted into patchpoints and processed by the multiple shooting differential corrector described in Section 2.5. Table 3 displays the results of the differential correction process, comparing the states of the patchpoints before and after the process. One can see that the differential corrector adjusted each patchpoint away from the *x*-axis in order to produce a continuous trajectory, however, none of the patchpoints moved far. In this example, the differential corrector achieved a

Table 1
The eight states shown in Fig. 9.

State	Units	x	y	$\dot{x}$	$\dot{y}$
A: $\mathbf{X}^{+}_{LL_1-LL_1}$	Normalized	0.812255	0.0	0.0	0.248312
	SI (km, m/s)	312,230	0.0	0.0	254.418
B: $\mathbf{X}^{-}_{LL_1-LL_1}$	Normalized	0.878585	0.0	0.0	−0.281719
	SI (km, m/s)	337,728	0.0	0.0	−288.647
C: $\mathbf{X}^{+}_{LL_1-DPO}$	Normalized	0.813049	0.0	0.0	0.247532
	SI (km, m/s)	312,536	0.0	0.0	253.618
D: $\mathbf{X}^{-}_{LL_1-DPO}$	Normalized	0.890940	0.0	0.049050	−0.311179
	SI (km, m/s)	342,477	0.0	50.256	−318.830
E: $\mathbf{X}^{+}_{DPO-DPO}$	Normalized	1.061692	0.0	0.0	0.403877
	SI (km, m/s)	408,115	0.0	0.0	413.809
F: $\mathbf{X}^{-}_{DPO-DPO}$	Normalized	0.909845	0.0	0.0	−0.386264
	SI (km, m/s)	349,745	0.0	0.0	−395.762
G: $\mathbf{X}^{+}_{DPO-LL_1}$	Normalized	1.056340	0.0	0.0	0.432104
	SI (km, m/s)	406,057	0.0	0.0	442.729
H: $\mathbf{X}^{-}_{DPO-LL_1}$	Normalized	0.890940	0.0	−0.049050	−0.311179
	SI (km, m/s)	342,477	0.0	−50.256	−318.830

The state coordinates are given in the Earth–Moon synodic reference frame, relative to the Earth–Moon barycenter, in both non-dimensional normalized units and SI units.

Table 2
Two sequences that may be used as inputs to a differential corrector in order to produce continuous trajectories with different example itineraries.

Sequence	Objective	Sequence	Objective
A	Traverse LL_1	A	Traverse LL_1
B		B	
C	Transfer to DPO	C	Transfer to DPO
D		D	
E	Traverse DPO (1)	G	Transfer to LL_1
F		H	
E	Traverse DPO (2)	C	Transfer to DPO
F		D	
G	Transfer to LL_1	E	Traverse DPO
H		F	

The letters correspond to the states summarized in Fig. 9.

trajectory that met the requested continuity tolerances: the largest position and velocity discontinuities that were observed in any of the patchpoints along the final trajectory were $<0.4\,\text{mm}$ and $3.1\times10^{-9}\,\text{m/s}$, respectively.

4.2. Complex periodic orbits

A complex periodic orbit may be constructed by repeating a given sequence of states *ad infinitum* and inputting that theoretical sequence into the differential corrector. For instance, the following sequence may be used to represent a periodic orbit that consists of two revolutions about the LL_1 Lyapunov orbit, followed by one revolution about the distant prograde orbit, repeating itself indefinitely, where the orbits and letters are defined in Fig. 9

$$\{\ldots,\underbrace{A,B,A,B,C,D,G,H}\,,\underbrace{A,B,A,B,C,D,G,H}\,,\ldots\} \tag{10}$$

Fig. 10 shows a plot of such a periodic orbit. One can see that a trajectory following a complex itinerary gets very close to one of its generating three-body orbits even with as few as two revolutions about the orbit.

Since each unstable three-body orbit exists in a family, where the characteristics of each orbit in the family vary continuously from one end of the family to the other, it is hypothesized that a complex periodic orbit also exists in a family. The family of any given periodic orbit is limited in extent to some range of parameters [5]. The extent of the family of complex orbits is also limited in extent and it is hypothesized that the family may only extend through a range where each of its fundamental orbits and orbit transfers exists. Fig. 11 shows several example complex periodic orbits that exist in the same family as the orbit shown in Fig. 10. Each of these orbits has a different Jacobi constant, but the same morphology.

4.3. Generalization

The method demonstrated here has been illustrated by a very straight-forward example, namely, the construction of orbit transfers between an LL_1 Lyapunov orbit and a distant prograde orbit, two simple periodic three-body orbits. These orbits have been used because they are easily visualized and may be characterized using only a handful of states. Each state is placed at an x-axis crossing, although one can see in Table 3 that the states may be displaced during the differential correction process.

This method may certainly be applied to orbit transfers between other unstable three-body orbits, including non-symmetric orbits. In addition, a chain of orbits may certainly contain more than two different three-body orbits. Longer orbits and orbit transfers will likely require more states per segment for the differential corrector to converge. In that case, it is easier to visualize the problem by defining a sequence of states per segment and using symbols that represent sequences rather than individual states. Table 4 provides an example where the states A–H given above have been mapped to four such sequences.

If one refers to Fig. 6 from Section 3, one notices that there are two low-energy transfers between the example Lyapunov orbits about LL_1 and LL_2. One may construct a different sequence of states for each of those transfers, e.g., $\mathbf{S}^{1}_{LL\,1-LL\,2}$ and $\mathbf{S}^{2}_{LL\,1-LL\,2}$, which may be constructed from three or more states, including an initial state and two intermediate states in order to keep the trajectory segment lengths short enough to permit the differential corrector to converge.

Fig. 7 shows several low-energy transfers that exist from an orbit about LL_1 to an orbit about LL_2 that were

Table 3
The results of a differential correction process that converted the first sequence presented in Table 2 into a continuous trajectory.

Patchpoint		Initial state				Final state			
		x (km)	y (km)	$\dot{x}$ (m/s)	$\dot{y}$ (m/s)	x (km)	y (km)	$\dot{x}$ (m/s)	$\dot{y}$ (m/s)
A:	$\mathbf{X}^{+}_{LL_1-LL_1}$	312,230	0.0	0.0	254.418	312,242	0.000	0.000	254.092
B:	$\mathbf{X}^{-}_{LL_1-LL_1}$	337,728	0.0	0.0	−288.647	337,704	−0.003	0.034	−288.236
C:	$\mathbf{X}^{+}_{LL_1-DPO}$	312,536	0.0	0.0	253.618	312,399	0.640	1.180	253.675
D:	$\mathbf{X}^{-}_{LL_1-DPO}$	342,477	0.0	50.256	−318.830	342,553	12.782	51.463	−319.032
E:	$\mathbf{X}^{+}_{DPO-DPO}$	408,115	0.0	0.0	413.809	407,079	19.004	6.862	427.761
F:	$\mathbf{X}^{-}_{DPO-DPO}$	349,745	0.0	0.0	−395.762	349,595	−0.175	1.079	−393.771
E:	$\mathbf{X}^{+}_{DPO-DPO}$	408,115	0.0	0.0	413.809	408,081	0.000	0.000	414.071
F:	$\mathbf{X}^{-}_{DPO-DPO}$	349,745	0.0	0.0	−395.762	349,595	2.644	−1.094	−393.772
G:	$\mathbf{X}^{+}_{DPO-LL_1}$	406,057	0.0	0.0	442.729	407,079	16.916	−7.171	427.755
H:	$\mathbf{X}^{-}_{DPO-LL_1}$	342,477	0.0	−50.256	−318.830	342,557	−12.750	−51.431	−319.076
A:	$\mathbf{X}^{+}_{LL_1-LL_1}$	312,230	0.0	0.0	254.418	312,555	0.000	0.000	254.418

The coordinates shown here are in the Earth–Moon synodic reference frame, relative to the Earth–Moon barycenter.

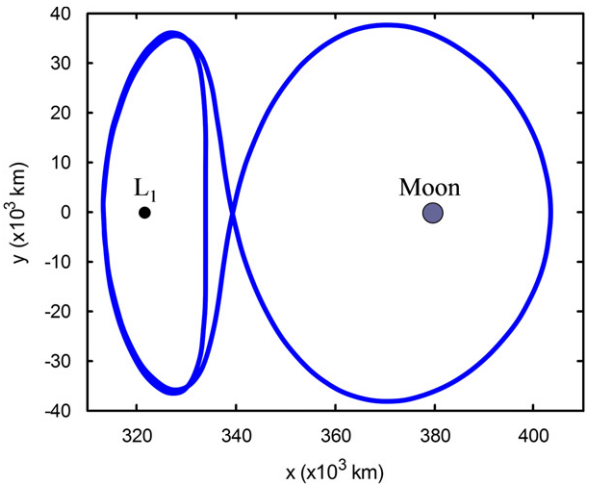

Fig. 10. A complex periodic orbit that consists of two revolutions about the LL_1 Lyapunov orbit, followed by one revolution about the distant prograde orbit, repeating itself indefinitely. This orbit is viewed from above in the Earth–Moon synodic reference frame.

generated using a Poincaré map. The transfer labeled (7) may be described as a complex chain that starts in an orbit about LL_1, transfers to a distant prograde orbit (DPO), remains in that orbit for a revolution, and then transfers from there to an orbit about LL_2. This complex chain was identified using a Poincaré map, but it may be quickly generated by differentially correcting the series of states represented by the following sequence:

$$\{\ldots,\mathbf{S}_{LL1},\mathbf{S}_{LL1},\mathbf{S}_{LL1-DPO},\mathbf{S}_{DPO},\mathbf{S}_{DPO-LL2},\mathbf{S}_{LL2},\mathbf{S}_{LL2},\ldots\} \tag{11}$$

5. Adding a maneuver to a transfer

The previous sections have explored orbit transfers that are entirely ballistic in nature. Such trajectories may be useful for scientific surveys of the near-Earth environment or to transfer assets from one orbit to another. Canalias et al. studied how a sequence of homoclinic transfers may permit a spacecraft to change its phase angle about an orbit without using any fuel, though it requires a lot of time [37]. Ballistic transfers represent a very small subset of the entire class of practical orbit transfers. It is not necessarily the case that the target orbit will have the same Jacobi constant as the initial orbit, or that the spacecraft is free to arrive at the target orbit at any phase angle in any duration of time. There are numerous reasons why it may be necessary to add one or more maneuvers to an orbit transfer. A particular case is examined in this section where each transfer requires one maneuver.

In general it requires two maneuvers to perform an arbitrary orbit transfer: one to depart the first orbit and one to arrive onto the target orbit. If the two orbits intersect in position-space within a desirable amount of time then it only requires a single maneuver to correct the velocity change at that intersection. The unstable and stable manifolds of unstable three-body orbits provide useful extensions to their host orbits, permitting more intersections to occur. Such intersections are much more prevalent in the planar CRTBP than in the three-dimensional CRTBP, though the results are still representative of many three-dimensional transfer problems. This discussion will restrict itself to the study of planar orbit transfers that require only a single maneuver.

5.1. Transfer problem formulation

It will be assumed that the cost of diverting away from the initial orbit onto its unstable manifold is trivial, the cost of arriving at the final orbit from its stable manifold is trivial, and the cost of performing a transfer from the point τ^U along the initial orbit to the point τ^S along the final orbit is the least-expensive intersection of the two resulting manifold trajectories.

This single-maneuver method has been applied to the problem of a spacecraft transferring between the two Lyapunov orbits used in this paper, namely, the Lyapunov orbit about LL_1 and the Lyapunov orbit about LL_2 that each have a Jacobi constant of 3.13443929. The spacecraft

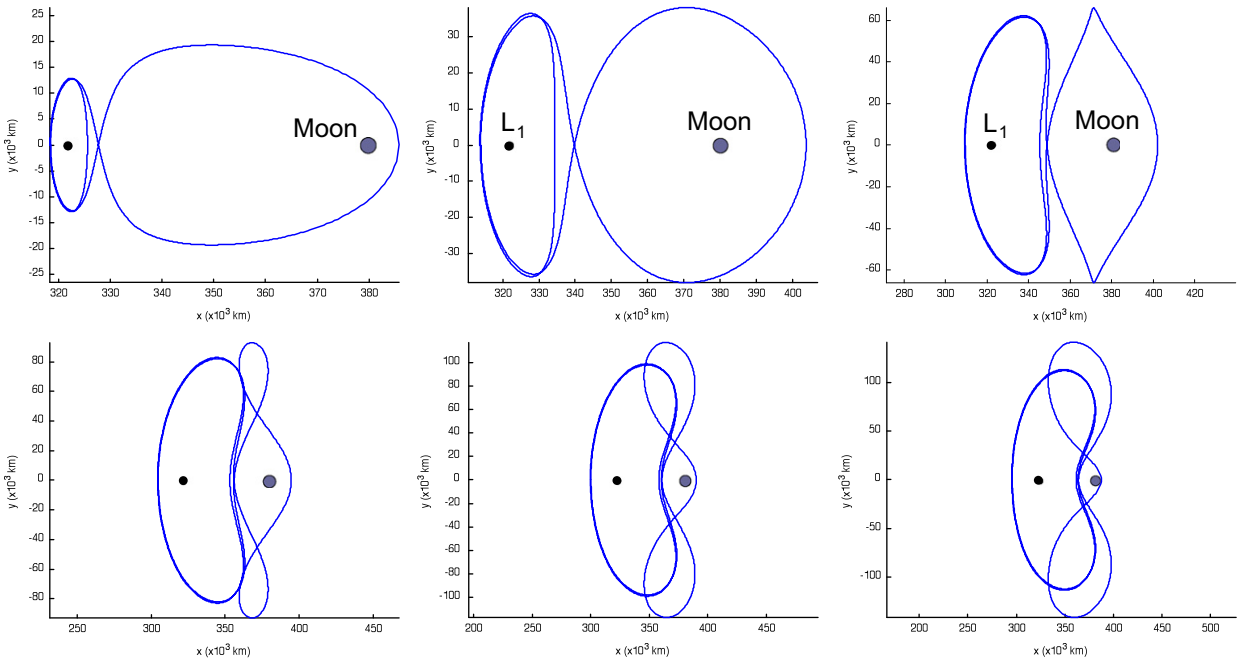

Fig. 11. Several example complex periodic orbits that exist in the same family as the orbit shown in Fig. 10.

Table 4
The mapping of the states A–H to sequences.

Sequence	States	Purpose
$\mathbf{S}_{LL\ 1}$	{*A*, *B*}	Traverse the LL_1 orbit
$\mathbf{S}_{LL1-DPO}$	{*C*, *D*}	Transfer from LL_1 to DPO
$\mathbf{S}_{DPO}$	{*E*, *F*}	Traverse the DPO
$\mathbf{S}_{DPO-LL1}$	{*G*, *H*}	Transfer from DPO to LL_1

begins from each τ^U in a large set of values within the range $0 \leq \tau^U \leq 1$ and arrives at each τ^S in a similar set of values within the range $0 \leq \tau^S \leq 1$. The spacecraft's state at each given τ- value is perturbed in the direction of the stable or unstable eigenvector by a perturbation with a position magnitude of 100 km. At every (τ^U,τ^S) combination, the trajectories in both manifolds are propagated for a given amount of time, as specified below. If the two trajectories intersect in position-space, then the cost of the orbit transfer is determined to be the intersection that requires the least amount of ΔV. All propagation is performed by an eighth-order variable time-step Runge Kutta integrator [43] in the Earth–Moon CRTBP; in addition, a trajectory's propagation is terminated at any point where it impacts the surface of the Earth or of the Moon.

Fig. 12 shows a plot of the ΔV required to transfer from the LL_1 Lyapunov orbit at 500 evenly spaced τ^U values to the LL_2 Lyapunov orbit at 500 evenly spaced τ^S values, where the manifolds have been propagated for one month each. Thus, in this scenario, the maximum transfer duration is two months. One can see in Fig. 12 that most combinations of τ^U and τ^S result in transfers that require more than 100 m/s of ΔV. The combinations labeled "lunar collision" produce trajectories that both intersect the surface of the Moon before intersecting. Fig. 13 shows the three free transfers that are observed in Fig. 12, as well as three more expensive transfers. Table 5 provides quantitative information about the free transfers and several representative transfers that require a maneuver. One can see that the ΔV cost of a transfer increases quickly as either τ^U or τ^S moves away from a free transfer. In some cases, changing either τ^U or τ^S causes the trajectories to intersect in a new way or prevents them from intersecting in the same manner, resulting in an abrupt shift in the ΔV cost of the transfer. The duration of a transfer is defined as the time it takes to traverse from the point τ^U to the point τ^S.

Fig. 14 shows a similar plot as that shown in Figs. 12 and 13, but in this scenario the trajectories have been propagated for three months each. In this case, the longest transfer may take six months to complete. The grid includes 500 τ- values each. One can see that new (τ^U,τ^S) combinations appear in Fig. 14 that require less ΔV than their shorter-duration equivalents in Fig. 12. Fig. 15 shows a closer view of the plot in the range $0.92 \leq \tau^U \leq 1.08$ and $0.70 \leq \tau^S \leq 1.00$, in a grid with 230 evenly spaced τ- values, to observe more of the structure around longer orbit transfers. Fig. 16 and Table 6 provide several example trajectories of the available low-energy transfers. In general, the closer each (τ^U,τ^S) combination is to a free transfer, the smaller the ΔV requirement is for that transfer.

6. Discussion

The transfers studied here have been restricted to the planar three-body system. Three-dimensional orbits in

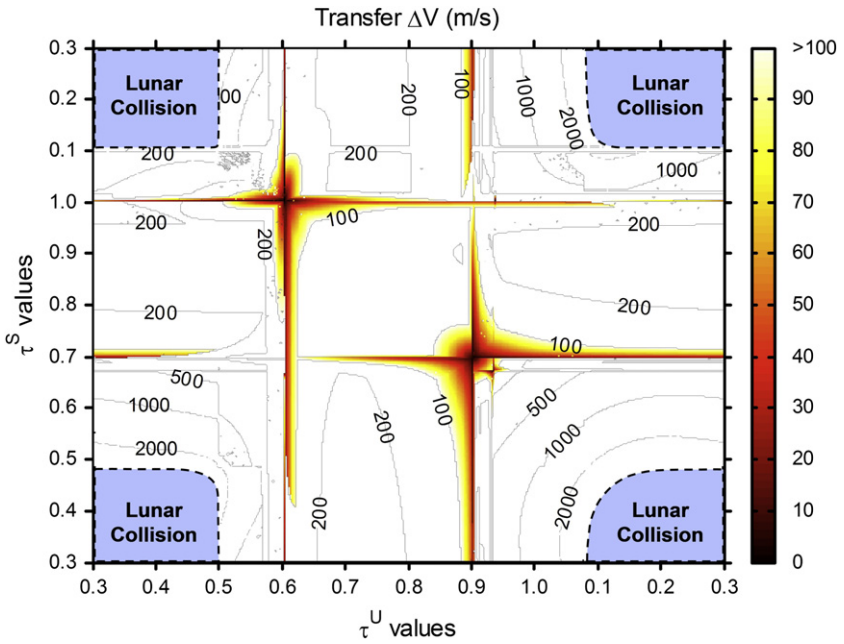

Fig. 12. The total ΔV required to transfer from the LL_1 Lyapunov orbit at any given $\tau = \tau^U$ value to the LL_2 Lyapunov orbit at any given $\tau = \tau^S$ value, where the manifolds have been propagated for one month each. The points colored black correspond to (τ^U, τ^S) combinations that yield a transfer that requires no deterministic ΔV.

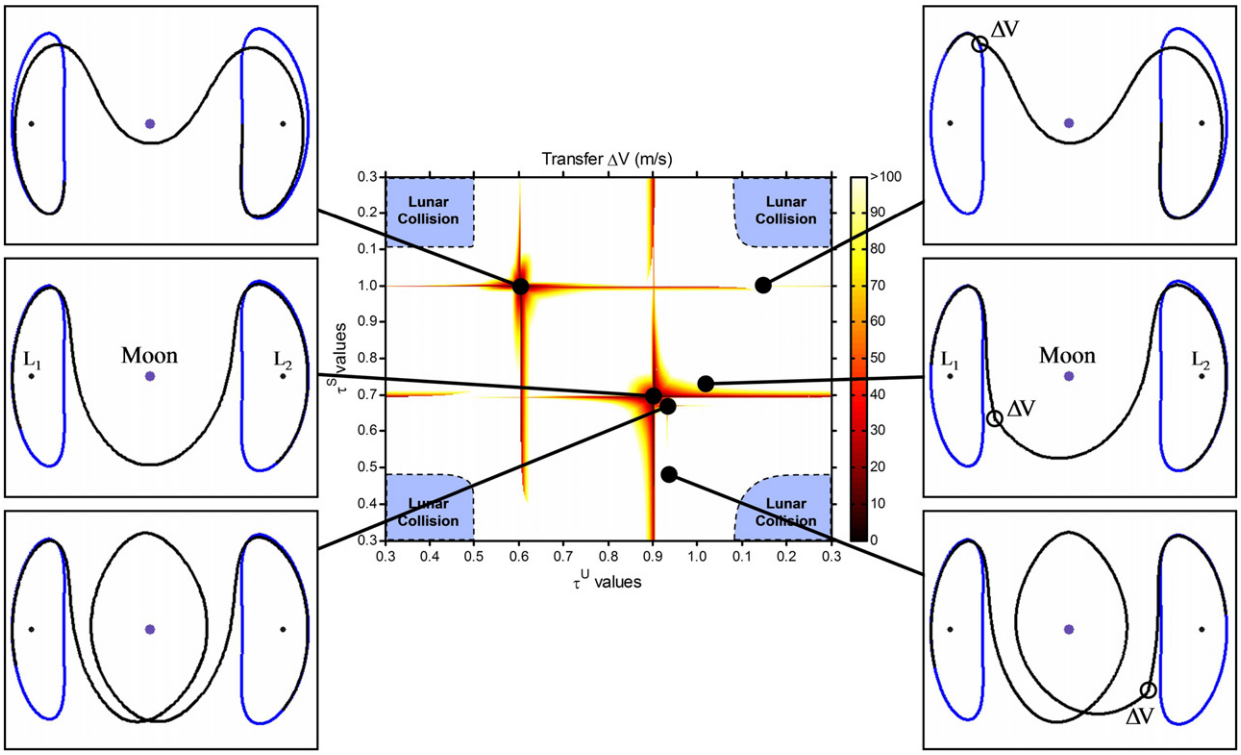

Fig. 13. The same ΔV plot shown in Fig. 12 with several example transfers shown. The three transfers shown on the left are free; the three shown on the right require a single maneuver.

the Earth–Moon system often have many practical advantages over planar orbits, including a reduction in the number and duration of eclipses, improved access from other three-dimensional orbits, and improved communication and navigation geometry, particularly when accessing locations like the lunar South Pole. Many of the

techniques studied in this paper become more difficult in the three-dimensional problem. For instance, Section 3 demonstrated that a heteroclinic connection between two unstable three-body orbits in the planar problem may be identified by observing the intersections of the unstable manifold of the first orbit with the stable manifold of the second orbit as those manifolds pierce a Poincaré surface of section. The manifolds of three-dimensional periodic orbits are less likely to intersect in the Poincaré surface due to the two additional degrees of freedom. The manifolds may not even intersect in position-space. If the two orbits' manifolds do not intersect in position-space in a timely fashion, and the orbits cannot be otherwise adjusted, then a transfer between them requires at least two maneuvers.

Table 5
The parameters for several transfers identified in Figs. 12 and 13.

τ^U	τ^S	ΔV (m/s)	Duration (days)
~0.60136	Any	0.0	23.73[a]
~0.90007	Any	0.0	22.75[a]
~0.93139	Any	0.0	32.80[a]
Any	~0.99968	0.0	23.73[a]
Any	~0.69462	0.0	22.75[a]
Any	~0.66866	0.0	32.80[a]
0.60136	0.99968	0.0	23.73
0.60160	0.99940	1.2	23.71
0.60200	0.99900	2.0	23.73
0.60500	0.99500	11.9	23.72
0.00000	0.69462	0.0	21.48
0.00000	0.69470	4.8	21.47
0.00000	0.69500	12.7	21.41
0.00000	0.69700	26.3	21.62
0.93139	0.48000	15.8	30.18
0.93130	0.48000	37.5	30.25
0.93120	0.48000	52.9	30.30
0.93110	0.48000	64.0	30.33
0.13000	0.99968	10.7	29.65
0.13000	0.99969	20.9	29.61
0.13000	0.99970	27.4	29.59
0.13000	0.99971	32.3	29.56

[a] The transfer duration corresponds to the duration of time that the spacecraft is beyond 100 km from either orbit.

7. Applications to mission designs

There are many applications of low-energy orbit transfers and complex periodic orbits to practical mission designs in the near-Earth environment. One of NASA's goals is to establish a permanent presence at the Moon. It is certainly a possibility that one or more spacecraft will be sent to three-body orbits to accomplish a part of this goal. The low-energy transfers and orbit chains presented in this paper may prove useful if a spacecraft needs to transfer from one three-body orbit to another.

Low-energy orbit transfers have been shown to be very useful to place several spacecraft into a constellation using a single launch [1]. By extension, it is possible to chain several three-body orbits together in order to place communication/navigation satellites in orbit about LL_1, LL_2, and the Moon using a single launch. In addition, mission designers may use similar low-energy transfers to reconfigure a constellation that has already been

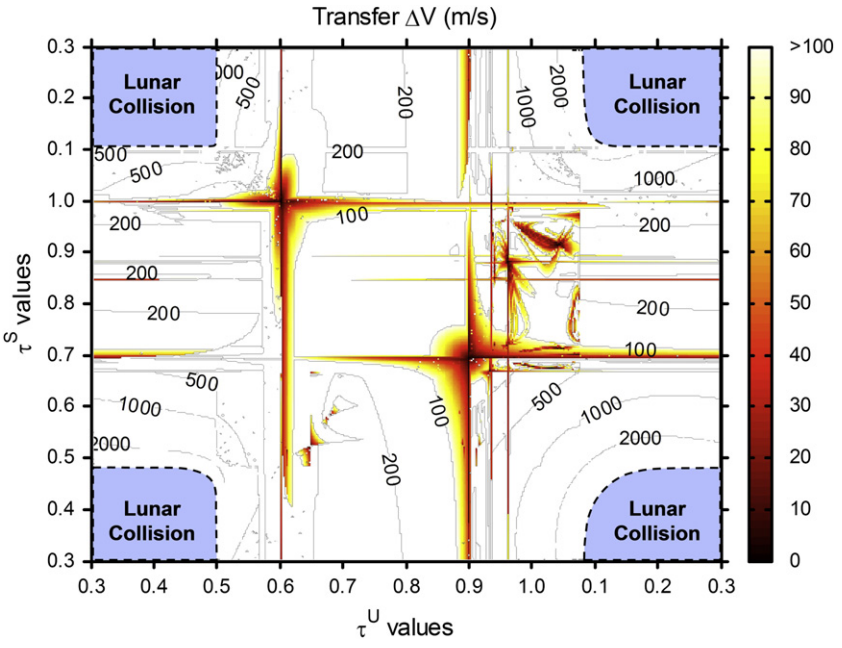

Fig. 14. The total ΔV required to transfer from the LL_1 Lyapunov orbit at any given $\tau = \tau^U$ value to the LL_2 Lyapunov orbit at any given $\tau = \tau^S$ value, where the manifolds have been propagated for three months each.

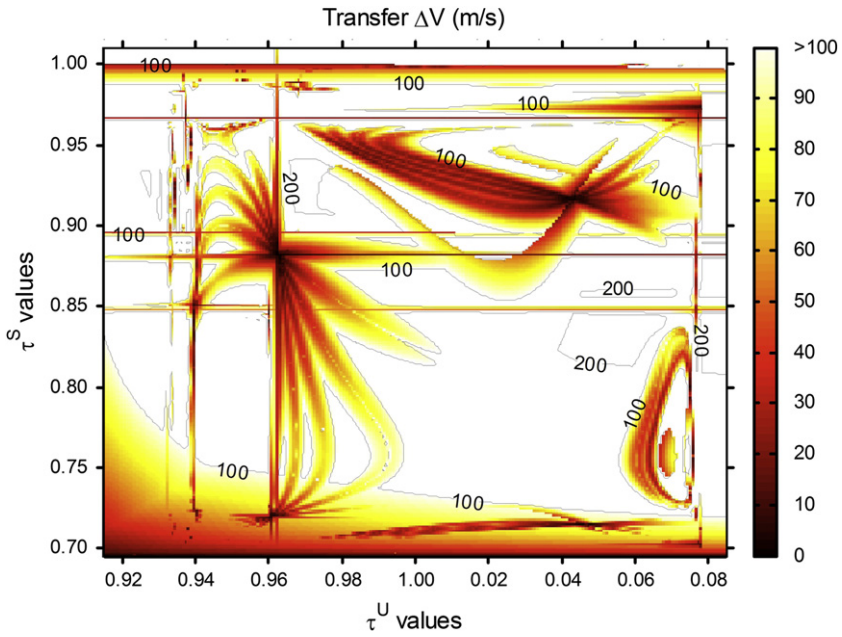

Fig. 15. The region of the plot shown in Fig. 14 in the range $0.92 \leq \tau^U \leq 1.08$ and $0.70 \leq \tau^S \leq 1.00$.

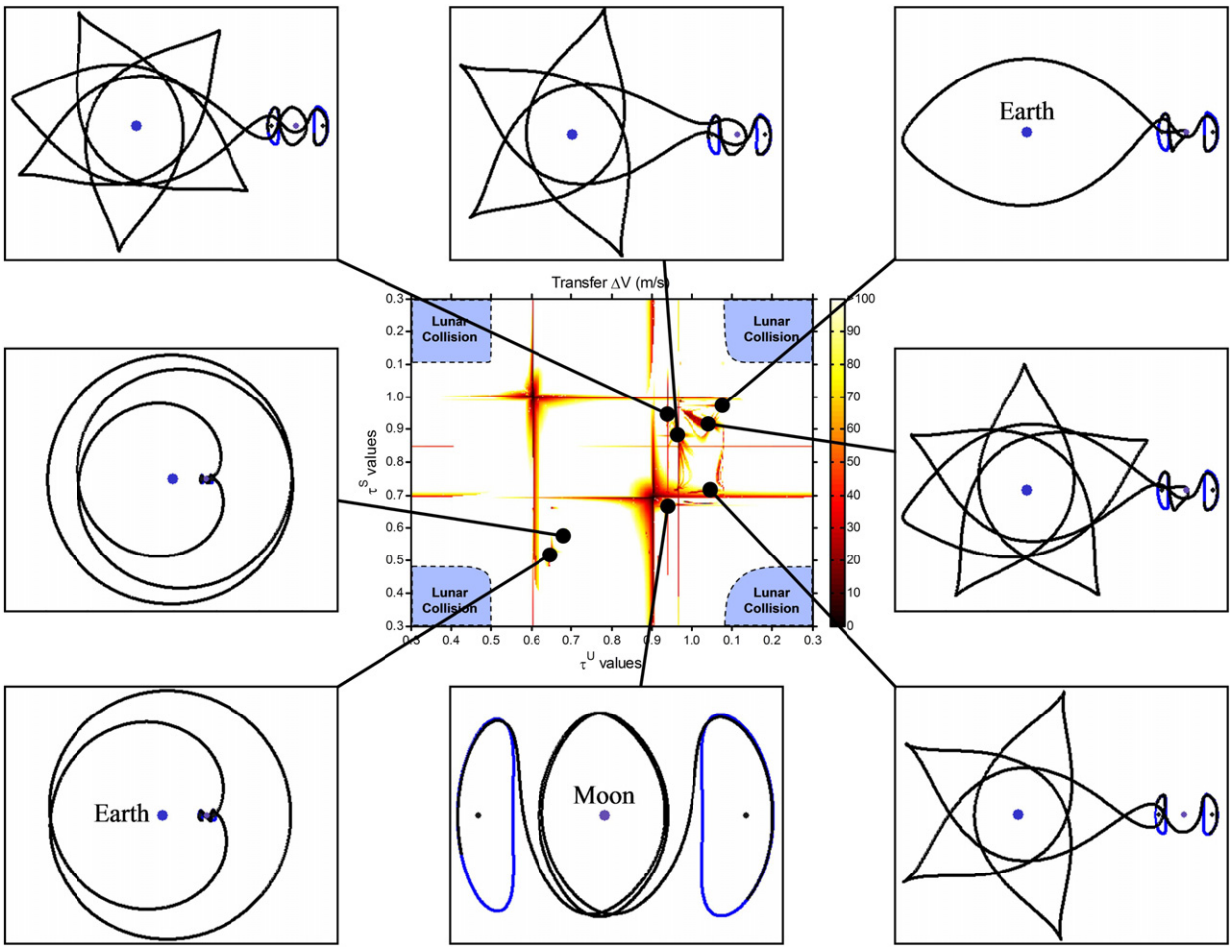

Fig. 16. The same ΔV plot shown in Fig. 14 with several example free transfers shown.

Table 6
The parameters for several free transfers identified in Figs. 14 and 16.

τ^U	τ^S	Transfer duration (days)
Orbit transfers with a duration between 0 *and* 1 *month*		
~0.90007	~0.69462	22.75
~0.60136	~0.99968	23.73
Orbit transfers with a duration between 1 *and* 2 *months*		
~0.93139	~0.66866	32.80
~0.07776563	~0.97266100	56.19
~0.07730318	~0.70129796	58.25
Orbit transfers with a duration between 2 *and* 3 *months*		
~0.96176428	~0.88282439	85.75
~0.96144931	~0.88864900	85.76
~0.96036425	~0.71890504	87.32
~0.93935860	~0.85000447	88.13
~0.93969902	~0.72132639	89.29
Orbit transfers with a duration between 3 *and* 4 *months*		
~0.96445629	~0.67323001	95.03
~0.04529788	~0.71387580	111.80
~0.04622830	~0.71399807	111.81
~0.64746390	~0.52111094	112.78
~0.93788165	~0.93702706	115.54
~0.03128609	~0.67534386	118.78
~0.98605505	~0.67974991	119.06
~0.97844137	~0.68174930	119.41
Orbit transfers with a duration between 4 *and* 5 *months*		
~0.96792455	~0.98443114	124.87

Since each transfer is free, each may be constructed using either τ^U or τ^S.

established. For example, say there were several communication/navigation satellites in orbit about LL_1 and LL_2. If a spacecraft carrying humans were then sent to land on the far-side of the Moon, it would be very advantageous to be able to reconfigure the constellation and transfer those satellites in orbit about LL_1 to an orbit about LL_2. The reconfigured constellation would provide redundant communication and better navigation for the humans on the far-side of the Moon. After the humans departed the Moon, the constellation could be returned to its original configuration, or to an entirely different configuration, depending on the requirements at that time.

Other applications of low-energy orbit transfers to practical spacecraft missions include the design of rendezvous trajectories. It may be the case that a space station, or other scientific satellite, is in orbit about one of the Lagrange points and it requires service, replacement, or a replenishment of some consumable resource. Mission designers may construct a rendezvous trajectory using knowledge of the low-energy orbit transfers presented in this paper. Alternatively, a spacecraft carrying potentially dangerous cargo may be sent into a long-duration, three-body orbit as a quarantine orbit using low-energy transfers. Later, that spacecraft may rendezvous with another craft, or simply transfer out of the near-Earth vicinity using similar low-energy transfers.

8. Conclusions

In this paper, we have described methods to construct orbit transfers, chains, and complex periodic orbits in the planar CRTBP using the invariant manifolds of unstable three-body orbits. The technique may be used to construct a trajectory that is free of deterministic maneuvers for a spacecraft to transfer between orbits about the Earth–Moon L_1 point, the L_2 point, and other orbits about the system. This study has been focused on trajectories in the Earth–Moon system; however, the technique may certainly be applied to other three-body systems.

The method described in this paper constructs complex trajectories out of fundamental periodic orbits and their homoclinic and heteroclinic connections. A Poincaré map has been used to identify the states along homoclinic and heteroclinic orbit transfers and a multiple shooting differential corrector has been used to adjust the states to make each trajectory continuous. Several example itineraries have been studied to demonstrate the technique, including transfers between an orbit about the Earth–Moon L_1 point and a prograde orbit about the Moon. The method has also been used to generate many orbits within a family of complex periodic orbits.

These low-energy transfers are particularly good when a spacecraft's mission is flexible enough to follow the natural dynamics in the system. In many situations the spacecraft must perform at least one maneuver to execute a desirable orbit transfer. This paper has explored the ΔV cost and time duration needed to perform one-maneuver transfers from any given state along one libration orbit to any given state along another libration orbit in the Earth–Moon three-body system. Many example transfers have been constructed and surveyed. It has been shown that a spacecraft requires substantially less ΔV to perform a single-maneuver transfer if the transfer is near a free transfer in the corresponding phase space.

Complex orbit transfers have many applications in practical spacecraft missions. This research demonstrates how to construct an arbitrarily complex series of orbit transfer using basic information about simple orbits that exist in the Earth–Moon system.

Acknowledgments

This work has been completed under partial funding by a NASA Graduate Student Researchers Program (GSRP) Fellowship by the National Aeronautics and Space Administration through the Jet Propulsion Laboratory, California Institute of Technology, by a National Science Foundation Graduate Research Fellowship, by a Zonta International Amelia Earhart Fellowship, and by funds from the Alliance for Graduate Education and the Professoriate.

References

[1] K. Hill, J.S. Parker, G.H. Born, N. Demandante, A lunar L2 navigation, communication, and gravity mission, in: AIAA/AAS Astrodynamics Specialist Conference, AIAA 2006-6662, AIAA/AAS, Keystone, Colorado, 2006.

[2] K. Hill, G.H. Born, Autonomous interplanetary orbit determination using satellite-to-satellite tracking, AIAA Journal of Guidance, Control, and Dynamics 30 (3) (2007).
[3] K. Hamera, T. Mosher, M. Gefreh, R. Paul, L. Slavkin, J. Trojan, An evolvable lunar communication and navigation constellation concept, in: IEEE Aerospace Conference, IEEE 1491, IEEE, Big Sky, Montana, 2008.
[4] V. Szebehely, Theory of Orbits: The Restricted Problem of Three Bodies, Academic Press, New York, 1967.
[5] J.S. Parker, Low-energy ballistic lunar transfers, Ph.D. Thesis, University of Colorado, Boulder, Colorado, 2007.
[6] D.A. Vallado, Fundamentals of Astrodynamics and Applications, second ed., Published jointly by Microcosm Press, El Segundo, CA, and Kluwer Academic Publishers, Dordrecht/Boston/London, 2001.
[7] G. Gómez, W.S. Koon, M.W. Lo, J.E. Marsden, J. Masdemont, S.D. Ross, Invariant manifolds, the spatial three-body problem and space mission design, in: AIAA/AAS Astrodynamics Specialist Meeting, AIAA 01-301, AIAA/AAS, Quebec City, Canada, 2001.
[8] G.H. Darwin, Periodic orbits, Acta Mathematica 21 (1897) 99–242.
[9] E. Strömgren, Connaissance actuelle des orbites dans le problème des trios corps, Copenhagen Observatory Publications (100), also Bulletin Astronomique 9 (87) (1935).
[10] C.L. Goudas, Three dimensional periodic orbits and their stability, Icarus 2 (1963) 1–18.
[11] M. Hénon, Exploration Numérique du Problème des Trois Corps, (I), Masses Egales, Orbites Périodiques, Annales d'Astrophysique 28 (3) (1965) 499–511.
[12] M. Hénon, Exploration Numérique du Problème des Trois Corps, (II), Masses Egales, Orbites Périodiques, Annales d'Astrophysique 28 (6) (1965) 992–1007.
[13] M. Hénon, Exploration Numérique du Problème des Trois Corps, (III), Masses Egales, Orbites Non Périodiques, Bulletin Astronomique 1 (1) (1966) 57–80.
[14] M. Hénon, Exploration Numérique du Problème des Trois Corps, (IV), Masses Egales, Orbites Non Périodiques, Bulletin Astronomique 1 (2) (1966) 49–66.
[15] M. Hénon, Numerical exploration of the restricted problem. V. Hill's case: periodic orbits and their stability, Astronomy & Astrophysics 1 (1969) 223–238.
[16] T.A. Bray, C.L. Goudas, Doubly-symmetric orbits about the collinear lagrange points, The Astronomical Journal 72(2).
[17] R.A. Broucke, Periodic orbits in the restricted three-body problem with Earth–Moon masses, Technical Report 32-1168, Jet Propulsion Laboratory, California Institute of Technology, 1968.
[18] R.W. Farquhar, The control and use of libration-point satellites, Ph.D. Thesis, Department of Aeronautics and Astronautics, Stanford University, Stanford, CA, 1968.
[19] J.V. Breakwell, J.V. Brown, The Halo family of 3-dimensional periodic orbits in the Earth–Moon restricted 3-body problem, Celestial Mechanics 20 (1979) 389–404.
[20] K.C. Howell, Three-dimensional, periodic, 'halo' orbits, Celestial Mechanics 32 (1) (1984) 53–71.
[21] K.C. Howell, H.J. Pernicka, Numerical determination of lissajous trajectories in the restricted three-body problem, Celestial Mechanics 41 (1988) 107–124.
[22] G. Gómez, J. Masdemont, C. Simó, Quasihalo orbits associated with libration points, The Journal of the Astronautical Sciences 46 (2) (1998) 135–176.
[23] S.H. Strogatz, Nonlinear Dynamics and Chaos, Perseus Books Publishing, L.L.C., Cambridge, MA, 1994.
[24] D.P. Muhonen, Accelerometer-enhanced orbit control near the Sun–Earth L_1 libration point, in: AIAA 21st Aerospace Sciences Meeting, AIAA-83-0018, AIAA, Reno, Nevada, 1983.
[25] M. Limon, et al., Wilkinson microwave anisotropy probe (WMAP): explanatory supplement, Technical Report 1.0, Goddard Space Flight Center, NASA/GSFC, Greenbelt, MD, 2003.
[26] N.G. Smith, K.E. Williams, R.C. Wiens, C.E. Rasbach, Genesis—the middle years, IEEE Aerospace Conference, IEEE, vol. 1, Big Sky, Montana, 2003.
[27] K.E. Williams, G.D. Lewis, R.S. Wilson, C.E. Helfrich, C.L. Potts, Genesis Earth return: refined strategies and flight experience, in: AAS/AIAA Space Flight Mechanics Conference, AAS 05-116, AAS/AIAA, Copper Mountain, CO, 2005.
[28] S. Wiggins, Introduction to Applied Nonlinear Dynamical Systems and Chaos, Text in Applied Mathematics, vol. 2, Springer-Verlag, New York, 1990.
[29] G. Gómez, W.S. Koon, J.E. Marsden, J. Masdemont, S.D. Ross, Connecting orbits and invariant manifolds in the spatial restricted three-body problem, Nonlinearity 17 (5) (2004) 1571–1606.
[30] S.D. Ross, Cylindrical manifolds and tube dynamics in the restricted three-body problem, Ph.D. Thesis, California Institute of Technology, 2004.
[31] G. Gómez, A. Jorba, A. Masdemont, C. Simó, Study of the transfer between halo orbits, Acta Astronautica 43 (9–10) (1998) 493–520.
[32] W.S. Koon, M.W. Lo, J.E. Marsden, S.D. Ross, Heteroclinic connections between periodic orbits and resonance transitions in celestial mechanics, Chaos 10 (2) (2000) 427–469.
[33] K.C. Howell, B.T. Barden, M.W. Lo, Application of dynamical systems theory to trajectory design for a libration point mission, Journal of the Astronautical Sciences 45 (2) (1997) 161–178.
[34] R.P. McGehee, Some homoclinic orbits for the restricted three body problem, Ph.D. Thesis, University of Wisconsin, Madison, Wisconsin, 1969.
[35] E.A. Belbruno, B.G. Marsden, Resonance hopping in comets, The Astronomical Journal 113 (4) (1997) 1433–1444.
[36] D. Wilczak, P. Zgliczyński, Heteroclinic connections between periodic orbits in planar restricted circular three body problem. Part II, Communications in Mathematical Physics 259 (3) (2005) 561–576.
[37] E. Canalias, A. Delshams, J.J. Masdemont, P. Roldán, The scattering map in the planar restricted three body problem, Celestial Mechanics and Dynamical Astronomy 95 (2006) 155–171.
[38] E. Canalias, J.J. Masdemont, Homoclinic and heteroclinic transfer trajectories between Lyapunov orbits in the Sun–Earth and Earth–Moon Systems, Discrete and Continuous Dynamical Systems 14 (2006) 261–279.
[39] M.W. Lo, S.D. Ross, SURFing the solar system: invariant manifolds and the dynamics of the solar system, Technical Report, Jet Propulsion Laboratory, California Institute of Technology, 1997.
[40] R. Wilson, Derivation of differential correctors used in GENESIS mission design, Technical Report JPL IOM 312.I-03-002, Jet Propulsion Laboratory, California Institute of Technology, 2003.
[41] T.S. Parker, L.O. Chua, Practical Numerical Algorithms for Chaotic Systems, Springer-Verlag, New York, 1989.
[42] C. Robinson, Dynamical Systems: Stability, Symbolic Dynamics, and Chaos, second ed., CRC Press, LLC, 2000 Corporate Blvd., N.W., Boca Raton, FL 33431, 1999.
[43] H. Wilson, L. Turcotte, Advanced Mathematics and Mechanics Applications Using MATLAB, second ed., CRC Press, Boca Raton, Florida, 1997.